Experimental and Analytical Behavior of Short Concrete Columns Reinforced with GFRP Bars under Eccentric Loading

Koosha Khorramian[1] and Pedram Sadeghian[2]

ABSTRACT: This paper presents experimental and analytical studies on short concrete columns reinforced with glass fiber-reinforced polymer (GFRP) towards characterizing compressive behavior GFRP bars. The experimental program consisted of fourteen 500 mm-long specimens with a square cross-section (150x150 mm) including nine GFRP reinforced (6#5) and five plain concrete specimens. The specimens were tested under concentric and eccentric compressive load up to failure. Three eccentricity to width ratios of 0.1, 0.2, and 0.3 were considered, where the eccentricities applied symmetrically at both ends of simply supported columns. The experimental program showed no crushing of GFRP bars at peak load and the corresponding strain did not reach 50% of their crushing capacity obtained from material test. In addition, an analytical model was developed and verified against the experimental test data. The model considered both material nonlinearity and geometrical nonlinearity. Using the model, a parametric study was performed on the effect of eccentricity, reinforcement ratio, and concrete strength, which confirmed the capability of GFRP bars to sustain high strains without reaching the compressive strain capacity of the bars. The study showed that GFRP bars can be considered as load bearing longitudinal reinforcement of concrete columns and ignoring their effect is not necessary.

KEYWORDS: GFRP, Column, Concrete, Crushing, Test, Model.

---

[1] PhD Student, Department of Civil and Resource Engineering, Dalhousie University, D301, 1360 Barrington street, Halifax, NS, B3H 4R2 Canada, koosha.khorramian@dal.ca
[2] Assistance Professor and Canada Research Chair in Sustainable Infrastructure, Department of Civil and Resource Engineering, Dalhousie University, B233B, 1360 Barrington Street, Halifax, NS, B3H 4R2 Canada, Pedram.Sadeghian@dal.ca (corresponding author)

1. INTRODUCTION

Fiber-reinforced polymer (FRP) composite bars have been used in construction industry as an alternative to steel reinforcing bars (rebars) in concrete structures where high corrosion resistance is needed [1]. Moreover, glass FRP (GFRP) have a unique electromagnetic transparency which makes them suitable for applications where electromagnetic fields are recognized as critical design criterion [2]. There have been many investigations on the behavior of GFRP bars in concrete beams [3, 4, 5], slabs [6, 7, 8], bridge decks [9, 10], and walls [11, 12]. As a result, the use of GFRP bars have become widespread in structural applications where bending capacity is needed. However, the application of GFRP bars in concrete columns has been limited, although multiple researchers performed different studies on GFRP bars in columns [13, 14, 15, 16, 17, 18, 19].

It is commonly believed that GFRP bars are not as effective as steel bars in load bearing capacity of concrete columns. For example, the ACI 440.1 [20] design guide for GFRP bars neglects the contribution of the GFRP bars in compression and allows the replacement of them with concrete in calculations. Another example is CAN/CSA S806 [21], Canadian standard for design and construction of building structures with GFRP, which allows the use of GFRP bars in concentrically loaded columns only if the designer neglects their contribution in strength. Furthermore, *fib* Bulletin 40 [22] mentioned that since the contribution of the compressive GFRP rebars to the load carrying capacity of concrete column is less than the steel rebars, their contribution is ignored.

Choo et al. [23] performed an analytical study on FRP reinforced concrete columns and mentioned that ignoring FRP rebars in the compression zone may be conservative, however, they have not checked the compressive strain of FRPs in compression to see whether compressive failure of FRPs occur or not. Also, De Luca et al. [2] tested large-scale concrete columns reinforced with GFRP bars under concentric compression and concluded that GFRP bars are more susceptible to instability since their compressive strength and stiffness in compression are less than in tension. On the other hand, Tobi et al. [24] showed the compressive strength of GFRP bars at peak load of concrete columns is 35% of their capacity in tension. They also reported that the contribution of GFRP bars were 10% of column capacity, which is close to steel bars' contribution (12%) which proves that GFRP bars could be used in columns where adequate confinement is provided. Hales et al. [16] conducted an experimental evaluation of slender high strength concrete columns reinforced with GFRP bars and found that GFRP spirals and longitudinal bars are a viable system of reinforcement for short and slender columns. Mohamed et al. [25] studied the performance of concrete columns reinforced with longitudinal FRP bars and determined that carbon FRP (CFRP) and GFRP bars experienced the compressive strain of 0.004 and 0.007 mm/mm which confirm that the compressive FRP bars are effective in load-carrying capacity of columns. Also, Khorramian and Sadeghian [26] and Fillmore and Sadeghian [27] experienced similar results in experimental investigation of concrete columns and observed that GFRP bars can sustain a significant level of compressive strains in columns.

As shown, the literature indicates that there are unknowns and controversial opinions regarding the behavior of GFRP bars in concrete columns. There are doubts about modulus and strength of GFRP bars in compression and the possibility of their premature crushing and/or buckling in concrete columns. Lack of standard method for testing GFRP bars in compression has also caused a gap of data regarding the corresponding mechanical properties. Thus, more research is needed to evaluate if there is a safety issue regarding compressive behavior of GFRP bars in concrete. Moreover, as considering an accidental load eccentricity is mandatory in column design, the compressive behavior of GFRP bars in concrete columns under combined axial load and bending moment needs to be investigated more in-depth to address their effectiveness for more realistic cases.

Since the contribution of FRP bars as longitudinal reinforcements of concrete columns has not been recognized by current design guidelines and their effects have been neglected, the industry and design engineers are skeptical of using FRP bars in compression, even ignoring their contribution. In addition, there is no standard test method for testing FRP bars in compression to establish a reliable data platform clarifying all unknown regarding compressive behavior of FRP bars. Manufacturers are also suffering from lack of a standard test method for evaluating the compressive behavior of their FRP products. Therefore, the motivation of this paper was to investigate the characteristics of FRP bars in compression where surrounded by concrete as well as proposing a simple coupon test method for testing FRP bars in compression. The results will help researchers, engineers, and manufacturers to understand better the behavior of FRP bars in compression.

This study focuses on the compressive behavior of GFRP bars in concrete columns under eccentric loading using both experimental and analytical methods for a selected square cross-section and GFRP rebar type which are explained in the following sections. In the experimental part, fourteen medium-scale GFRP reinforced concrete columns were tested under eccentric and concentric loads. In the analytical part, a model was developed and verified to mimic the behavior of the test columns and to perform a parametric study providing more information about the compressive behavior of GFRP reinforced concrete columns.

2. EXPERIMENTAL PROGRAM

The experimental program consisted of testing of GFRP reinforced concrete columns as well as plain ones under concentric and eccentric loads. The major test parameter was load eccentricity. This section starts with details of test matrix and material properties, followed by explanation of fabrication and test set up, and concluded by results and discussion.

2.1. Test Matrix

A total of fourteen 500 mm long concrete columns with a square cross section (150×150 mm) were prepared and tested under concentric and eccentric compressive loadings. Nine of these specimens were reinforced with six GFRP bars #5 (16 mm diameter). Four specimens consisting two plain concrete and two specimens reinforced with GFRP bars were tested under concentric axial load and other specimens were tested under eccentric loads at 15, 30, and 45 mm, i.e. 10, 20, and 30 percent of width of the cross-section, respectively. The test matrix is provided in Table 1. To name the specimens, a label like "A-ex-y" was used where A, x, and y indicate the column type (P or R), the eccentricity (e0, e10, e20, or e30), and the specimen number (1, 2, or 3), respectively. The column type is identified by "P" for plain (i.e. no reinforcement), or "R" for GFRP reinforced concrete columns. For example, "R-e10-1" means that it is the first specimen reinforced with GFRP rebar and tested under 10 percent eccentricity.

2.2. Material Properties

A ready-mix concrete with maximum aggregate size of 12.5 mm was used for making the concrete specimens. The concrete strength at the time of testing was 37.0±0.8 MPa by testing three concrete cylinders (100×200 mm). To reinforce the concrete specimens, six #5 sand coated GFRP bars with a diameter of 16 mm and nominal cross-sectional area of 197.9 mm^2 were used. To determine tensile characteristics of rebars, five tensile specimens were prepared and tested per ASTM

D7205M [28]. The mean and standard deviation of the tensile strength, tensile modulus, and ultimate tensile strain of rebars were evaluated as 629±30 MPa, 38.7±1.5 GPa, and 0.0162±0.0011 mm/mm, respectively. Figure 1(a) shows the stress-strain curves.

The compression properties of rebars were also examined by applying pure compression load on five short rebar specimens with a free length twice the diameter of rebars as shown in Figure 1(b). In order to eliminate the stress concentration and premature failure at the ends of rebar specimens, two steel caps including a steel hollow cylindrical section with inner diameter of 32 mm and depth of 12.7 mm were used. The caps were filled with a high strength epoxy-based grout to fix the rebar specimens. For the compression test, a spherical platen was used at the bottom of the specimens to align them with the axis of loading minimizing accidental eccentricities. Mode of failure of rebars in compression test was crushing and no buckling observed during the test. The compression strength, compression modulus, and crushing strain of bars at peak were evaluated as 783±74 MPa, 41.2±1.2 GPa, and 0.0190±0.0017 mm/mm, respectively. It should be highlighted that there is no ASTM standard for the compression test.

Figure 1(a) also shows the stress-strain curve obtained from the compression and tension tests. Two strain gauges used at the center of the compression rebar specimens which were malfunctioned/broken before reaching the ultimate load. Therefore, in order to complete the stress-strain curves for compression specimens, the values of stroke divided by a proper gauge length, which gives the tangent slope of the point at which strain gauge broke, were used as shown in Figure 1. The average of compression strains at which the strain gauges were broken was 0.0133 mm/mm called “proportional limit” for compression strains, before which the stress-strain curves are linear. The average proportional limit is 70% of the average crushing strain of 0.0190 mm/mm.

Moreover, the corresponding stress to the proportional limit was 534 MPa which was 68% of the average crushing stress (783 MPa).

It was observed that the modulus of elasticity of GFRP rebar tested in compression and tension are close to each other. Thus, the assumption of having the same modulus of elasticity in tension and compression is rational and it can be used to model the behavior of GFRP bars. The other observation is the comparatively higher crushing strength of GFRP in compression than its rupture strength in tension. Thus, ignoring compressive strength of GFRP bars and considering their strength and modulus like concrete in compression per ACI 440.1R [20] is too conservative. Since there is no standard method for testing FRP bars in compression, different values for the compressive strength have been reported. De Luca et al. [2] reported reductions in the compressive strength and elastic modulus of GFRP bars by up to 45 and 20% with respect to the values in tension, respectively. On the other hand Khan et al. [29] tested FRP bars both in compression and tension and the results showed considerably higher modulus and strength of tensile tests in comparison to compression tests while Mallick [1] referred to the typical mechanical properties of different laminas which shows lower, equal, or higher compressive strength than tensile ones depend on their type. Overall, the performance of GFRP bars in concrete could be different than coupon test. That is another reason for designing the experimental program.

2.3. Fabrication

Fresh concrete was casted in wooden molds which was prepared to hold the bars, and the movement of rebar was restricted by two wooden plates with holes, as shown in Figure 2(a), that were attached to the end of the mold as presented in Figure 2(b). The cover of GFRP rebar was selected as 25.4 mm in each direction which is consistent with available specifications for FRP rebar [20]. The center to center distance between two bars was 41.6 mm, and the distance from the edge of concrete to the center of rebar was 33.4 mm. There were two rows of rebar that each of them consisted of three rebar as is shown in Figure 2(a). The specimens were casted in one batch as shown in Figure 2(c), and were cured at room temperature by covering with plastic sheets to prevent losing the moisture as presented in Figure 2(d). In this experimental program, no tie was applied to the column specimens because of the scale of tests. Since the shear loads are very small because of the size of specimens and symmetric load eccentricities, and the confinement effect was not target of this study, the only possible function of ties could be providing GFRP bars with less unbraced length and prevent premature buckling before the specimens reach their ultimate capacity. In fact, the specimens were designed to allow any possible buckling of GFRP bars especially after the peak load to observe the post peak behavior of the specimens. Since the load concentration at bottom and top of the specimens, where the load applied, was expected to cause a premature failure, both ends of concrete columns were strengthened with two layers of 50 mm wide unidirectional basalt fabric and epoxy resin. The surface of concrete was grinded at the location of basalt wraps before applying epoxy resin to provide roughness, and wet basalt fabrics stretched on the surface of concrete using hand to be fit to the edges and corners of specimens for end wrappings. The corners were not rounded. Then, the top and bottom surfaces were flattened using a grinder to provide a smooth surface at top and bottom of each specimen.

2.4. Test Set Up

In this study, the boundary condition was pin-pin, which allows rotation at end of column, and load applied with the same eccentricity at both ends of column. Thus, two symmetric steel caps were used at the end of columns to satisfy the boundary condition and loading condition, as shown in Figure 3. The steel cap consists of a notched, 30 mm thick steel plate welded on a rigid steel plate (250×250×10 mm). A steel cylinder with the same length of notch, lubricated with grease was put in contact with steel cap through notch which permits the rotation of the specimen during testing. In addition, the location of steel caps on steel plate was adjusted based on different eccentricity demands using weld. Moreover, four adjustable angle profiles were attached to the steel cap to restrict the column's sway and cause consistent end rotation of steel cap and specimen. To make the steel cap more integrated with the testing specimens, two plastic bags were filled with fresh quick set cement based grout and placed between the interface of steel caps, including the interior surface of adjustable angles and the top steel plate, and the end of concrete specimens, both at top and bottom of column.

To analyze the behavior of the specimens, the horizontal and vertical displacement of column as well as the strains at outer surface of bars were measured using a data acquisition system reading the data from strain gauges and linear variable differential transformers (LVDTs) at 0.1 sec. time steps, as shown in Figure 3. Vertical LVDTs (i.e. LVDT 1 and 2), with a gauge length of 100 mm, were applied to secure enough data in case of malfunctioned strain gauges. Furthermore, two horizontal LVDTs (i.e. LVDT 3 and 4) were aligned with the center of concrete columns to measure the deflection of the mid-height of columns. The tests were performed by a 2 MN universal testing machine using a displacement control approach with a rate of 0.625 mm/min.

3. RESULTS AND DISCUSSION

A summary of the test results is shown in Table 2, in terms of the peak load (P_u), the strain of extreme compressive rebar at P_u and its ratio to proportional strain (i.e. 0.0133 mm/mm) and crushing strain (i.e. 0.0190 mm/mm) of GFRP coupons in compression. The table also shows the strain of extreme compressive rebar at $0.85P_u$ (post peak) and its ratio to proportional strain and crushing strain plus failure modes. In this section, the failure modes of test specimens and the effect of eccentricity on the load- displacement and the strain of GFRP bars are discussed.

3.1. Failure Mode

In this study, three modes of failure were detected including concrete crushing in compression (CC), concrete spalling in compression (CS), and concrete destruction (CD) as presented in Table 2. However, no buckling or crushing of GFRP bars were observed before the peak load. After peak load, some bars were locally buckled when the compressive concrete crushed and is not contributed to load bearing system. However, no crushing of GFRP bars were observed even after spalling of concrete and buckling of bars. The concrete crushing (CC) is defined as the state at which the strain at the extreme layer of compressive concrete reaches the strain of 0.003 mm/mm as is considered as the ultimate strain of concrete in compression by ACI 318 [30]. Most of time, crushing of concrete followed by the separation of concrete segments from the column which is defined as concrete spalling (CS). For nearly all eccentrically loaded specimens, the crushing and spalling of compressive concrete happened without crushing or buckling of bars as shown in Figure 4. For 10 percent eccentricity ratio, the plain concrete specimens (P-e10 group) immediately destructed after the spalling and split in half, which is called concrete destruction (CD) in this paper. Overall, for GFRP reinforced specimens, no crushing of GFRP bars were observed after significant lateral deformations and tests were terminated for safety reason.

3.2. Effect of GFRP Bars on Load and Displacement Behavior

Table 2 shows the average peak load of each group of specimens. It shows that the average load capacity of plain specimens under pure axial load was 719.2 kN and it increased to 774.9 kN for GFRP reinforced specimens (i.e. 7.74% increase). At the eccentricity ratio of 0.1, the load capacity of plain specimens was 596.3 kN and it increased to 692.8 kN for GFRP reinforced specimens (i.e.

16% increase). This indicates that GFRP bars contributed to the load bearing capacity of the specimens. Figure 5(a) shows the axial load vs. lateral displacement of the GFRP reinforced specimens under 0.1, 0.2, and 0.3 eccentricities. The curves of two identical specimens for each eccentricity are presented. It is observed that as the eccentricity increases, the peak load decreases and the lateral displacement at peak load increases. Overall, the post peak behavior of the GFRP reinforced specimens shows a gradual descending branch without sudden drops which is compatible with the test observations indicated no crushing of GFRP bars.

3.3. Effect of Eccentricity on Strain of GFRP Rebars

Figure 5(b) shows the axial load vs. strain of GFRP bars under 0.1, 0.2, and 0.3 eccentricity ratios. The figure indicates, as the eccentricity ratio increased, the strain of GFRP bars at peak load increased. It also shows that GFRP bars sustained considerable level of strain at the compression side and the level of strains in GFRP bars were much less than their crushing strain obtained in coupon test, which means GFRP bars were stressed much less than their capacities in tension and compression. This is due to low modulus of GFRP bars. It should be noted that for one of specimens in group R-e20 shown in Figure 5(b), the strain in compressive rebar was not continued to the peak load while the strain in tensile side was continued to the peak load, which could be due malfunction of the strain gauge in the compression side. In addition, it is observed that for specimens tested under eccentricity to width ratio, both strain gauges attached to GFRP bars experience compressive strain up to failure due to the comparatively low eccentricity. However, after the peak load the tests continued since the displacement control approach used for these experiments and as a result as the stroke displacement increases, the strain at compressive side increases and to satisfy the equilibrium of the section, the depth of neutral axis and compressive area contracted which leads to recording tensile strains after peak load on the tensile side. Table

2 shows that when the eccentricity ratio increased from 0 to 0.3, the strain of GFRP bars at peak load increased from 0.00275 to 0.00361 mm/mm. The ratio of recorded strains to proportional limit (i.e. 0.0133 mm/mm) and crushing strain (i.e. 0.0190 mm/mm) from coupon tests were calculated and presented in table 2. As shown, at peak load, the average ratios to proportional limit and crushing strain were 0.23 and 0.16, respectively. It means GFRP bars at peak load of specimens had a significant distance to their ultimate strain.

In order to have a better idea about post peak behavior of the specimens, an ultimate condition was defined for the specimen at which the axial load was dropped 15 percent according to a study on combined axial and flexural loads performed by Hognestad [31]. The importance of studying the post peak behavior reveals once the failure of GFRP bars did not observed at the peak load. Therefore, expectation of failure phenomenon such as crushing and buckling tracked up to a certain load after crushing which is 85% after peak load, ($0.85P_u$) in this study. Table 2 provides the average ratios of GFRP bar strains at 0.85 of peak load to the proportional limit and crushing strain of the GFRP bars. The results reveal that, in average, the strain of GFRP bars in compression at 0.85 of peak load were 0.0048 mm/mm, about 0.36 and 0.25 of proportional limit and crushing strain of GFRP rebar, respectively. It means compressive GFRP bars did not reach their capacity in crushing. It is noted that no buckling at peak load were observed which leads to the conclusion that GFRP bars are reliable reinforcing bars in load carrying system at peak load. In addition, even after 15% drop of peak load, the average strain of compressive GFRP bars were just quarter of their crushing strain. It should be highlighted that the values of strain at 0.85 of peak load would be even less than 0.0048 mm/mm if lateral ties limited their susceptibility to local buckling. This also indicates that GFRP rebars should be considered different than steel rebars in design of concrete columns. The contribution of GFRP rebars is a function of their modulus and level of strain at the ultimate condition, rather than tensile/compressive strength of bar materials. In the next section, an analytical model is presented to consider the effect parameters such as reinforcement ratio and concrete strength which were not considered in the experimental program.

4. ANALYTICAL STUDIES

This section presents an analytical study to model the behavior of FRP reinforced concrete columns under eccentric loading. The model generates load-strain, moment-curvature, and load-displacement curves considering both material and geometrical nonlinearities using an iterative cross-sectional analysis in MATLAB software.

4.1. Model Description

The analytical model consists of a combination of cross-sectional analysis and second-order analysis which depends on column cross-section, rebar layout, material properties, length, load eccentricity, and boundary condition. The cross-section of a rectangular column consisting of n layers of GFRP rebar is presented in Figure 6(a). The cross-sectional area, the distance from the furthest compressive fiber, and the location of each rebar layer from the neutral axis are presented by "A", "d", and "y" in the figure, respectively. Moreover, the depth of neutral axis is shown by "C" and the plastic centroid is presented by "C_P". The sign convention is positive for compression zone and negative in tension zone. It is assumed that the perfect bond exists between the concrete and GFRP bars so that the stains profile is considered as a linear, continuous function through the section for both compressive and tensile sides as shown in Figure 6(b). In order to find lateral displacement of column, a moment-curvature relationship at each particular load is needed which is derived by assuming the strain at the furthest compressive fiber in the section, ε_c, and the depth of neutral axis, C, as shown in Figure 6, discretizing the section to concrete fibers, finding strains, stresses, and controlling the satisfaction of equilibrium, which is explained in the following. The strain at the location of each rebar layer or at the center of every concrete fiber is calculated by:

$$\varepsilon_i = \left(\frac{\varepsilon_c}{c}\right) y_i \tag{1}$$

where ε_i is strain of concrete or GFRP bar, and y_i is the location of GFRP layer, or concrete fiber as shown in Figure 6(a). Once the strains are determined, a proper stress-strain relationship for concrete and GFRP bars gives the stresses at each rebar layer or concrete fiber. This model considers the stress-strain relationship of concrete in compression proposed by Popovics [32] as follows:

$$f_c = \frac{f'_c(\frac{\varepsilon_c}{\varepsilon'_c})r}{r - 1 + (\frac{\varepsilon_c}{\varepsilon'_c})^r} \tag{2}$$

where ε_c is the strain of compressive concrete, and f_c is the corresponding stress of concrete, f'_c is the concrete compressive strength, and $E_c$is the compressive modulus of elasticity of concrete. In Equation 2, other parameters are considered as $\varepsilon'_c = 1.7\frac{f'_c}{E_c}$, $E_c = 4700\sqrt{f'_c}$, $r = \frac{E_c}{E_c - E_s}$, and $E_s = \frac{f'_c}{\varepsilon'_c}$, where the values of concrete strength and modulus of elasticity of concrete are in MPa. Since the purpose of this model is to determine the behavior of concrete columns around the peak load, the tensile strength of concrete and tension stiffening effect are neglected to simplify the model. The stress-strain relationship of GFRP bars were considered as a linear, elastic curve up to the crushing in compression or rupture in tension with the same modulus of elasticity for both tension and compression sides as follows:

$$f_f = E_f \varepsilon_f \tag{3}$$

where f_f is the stress of GFRP bar, E_f is the modulus of elasticity of bars, and ε_f the strain corresponding to the stress. Although the modulus of elasticity assumed the same, the strength in tension and compression are different. For each GFRP bar layer, the stress is evaluated using Equation 2, and the internal force corresponding to each GFRP layer is derived by multiplication of the cross-sectional area of all bars in that layer and the stress at the center of the layer. The concrete section is discretized to a number of fibers whose stress is evaluated at the center of each layer using Equation 1 and Equation 2. Then, the internal force of concrete derived by summation of forces in all fibers, which are obtained by multiplying the area of each fiber and its corresponding stress and considering the effects of bars in compression part, as follows:

$$F_c = \sum_{a \quad \bar{y}_{c_i} \geq 0} \frac{1}{2}\left(f_{c_i} + f_{c_{i+1}}\right) b \delta_y - \sum_{a \quad y_f \geq 0} \frac{1}{2}\left(f_{c_i} + f_{c_{i+1}}\right) A_f \tag{4}$$

where F_c is the concrete internal force, f_{c_i} and $f_{c_{i+1}}$ are concrete stresses at top and bottom of each concrete fiber, b is the width of section, δ_y is the height of each concrete fiber, $\bar{y}_{c_i}$ is the location of center of each concrete fiber from neutral axis, y_{f_i} is the location of compressive GFRP layer from neutral axis, and A_f is the cross-sectional area of each GFRP layer. The number of layers in compressive zone was changed by changing the neutral axis location. In this study, the compressive zone always was divided into layers with 0.25 mm height. Afterwards, the sum of all internal loads gives the total internal force, P_n, which is calculated as follows:

$$P_n = F_c + \sum F_f \tag{5}$$

where P_n is the sum of all internal forces, F_c is the internal force of concrete, and F_{fi} is the internal force of i^{th} layer of GFRP rebar. If the sum of internal forces is equal to the applied load, the equilibrium is satisfied, otherwise, the whole process must be repeated by changing the depth of neutral axis until the satisfaction of equilibrium.

Once the equilibrium of forces is satisfied, the sum of all internal moments about the neutral axis is calculated for concrete and GFRP layers. For each GFRP layer the internal moment is calculated as the internal force times the corresponding distance from neutral axis while the internal moment of concrete fibers from neutral axis is calculated by:

$$M_c = \sum_{a \quad \bar{y}_{c_i} \geq 0} \frac{1}{2}(f_{c_i} + f_{c_{i+1}}) b \delta_y \bar{y}_{c_i} - \sum_{a \quad y_f \geq 0} \frac{1}{2}(f_{c_i} + f_{c_{i+1}}) A_f \, y_{f_i} \tag{6}$$

where, M_c is the concrete internal moment and other parameters are the same as Equation 4. Since the moment of internal forces is calculated about the neutral axis while the load eccentricity is measured from the center of plastic, the eccentricity is derived using Equation 7. The corresponding bending moment, M_n, for a determined curvature, which is defined as the furthest compressive concrete fiber divided by the depth of neutral axis, is then derived by Equation 8.

$$e^* = \frac{M_c + \sum F_s \, y_s}{P_n} \quad , \quad e = e^* - c + c_p \tag{7}$$

$$M_n = P_n e \tag{8}$$

In the equations, M_n is the total internal moment, P_n is the total internal force, e is the eccentricity of internal force from the center of plastic, e^* is the load eccentricity from the neutral axis, C is the depth of neutral axis, C_P is the depth of center of plastic, as shown in Figure 6(c), and other parameters are defined earlier. The mentioned process is repeated for a certain load and different values of furthest compressive concrete strain to find different curvatures and corresponding moments which leads to building the moment-curvature diagram of a given load. In this study, the loading path is derived by assuming the curvature and, in turn, the deflected shape of the column as a sine function as follows:

$$\emptyset(x) = (\emptyset_m - \emptyset_0)s\ \frac{\pi}{L} + \emptyset_0 \tag{9}$$

where $\emptyset(x)$ is the curvature function of the column at the distance x from the bottom of the clumn, $\emptyset_m$ and $\emptyset_0$ are the curvatures at the middle and the bottom of the column, respectively, and L is the length of the column. White and Macgregor [33] implemented a sine shape function for the deflected shape of slender steel-reinforced concrete columns and derivation of moment magnification factor. In addition, the assumption of deflected shape as a sine function was adopted from Broms and Viest [34], Lloyd and Regan [35], Claeson and Gylltoft [36] for steel reinforced concrete columns which was later verified by Sadeghian et al. [37] for FRP-wrapped concrete columns. Recently, the sine function was implemented for externally bonded concrete columns with longitudinal FRP laminates [38]. Although Mirmiran et al. [39] used a half cosine function as the deflected shape of GFRP reinforced concrete columns, their model used only to predict the capacity of columns. The model presented in the current study predicts the load displacement, the loading path, strain of concrete and FRP rebars up to the peak load (ascending branch), and after peak load (descending branch) behavior of GFRP reinforced concrete columns, which includes post-buckling behavior of slender columns and the behavior of the columns after concrete crushing for short columns.

By applying the moment-area theorem and having the curvature function, the maximum deflection, δ_m, is derived in the form of Equation 10. By integration, Equation 10 is rewritten as Equation 11.

$$\delta_m = \int_0^{L/2} \emptyset(x) d \quad = (\emptyset_m - \emptyset_0)\int_0^{L/2} s \quad \frac{\pi}{L} d \quad + \int_0^{L/2} \emptyset_0\, d \tag{10}$$

$$\delta_m = \frac{L^2}{\pi^2}\emptyset_m + \emptyset_0\left(\frac{L^2}{8} - \frac{L^2}{\pi^2}\right) \tag{11}$$

At a certain load, by building the moment-curvature and assuming the deflected shape of the column as a sine shape, an iterative process is used to find the deflection of column at its mid-height which is illustrated in Figure 7. In this process, three nodes are considered, one at the mid-height of column and two at the ends of column. An initial value of deflection at mid-height of column is assumed and based on that value and the initial eccentricity, the total load eccentricity and in turn, the corresponding moments are computed. Afterward, by using the moment-curvature diagram of that specific load, and reading the points corresponding to the initial and mid-height eccentricities, the values of curvature at the end of column, $\emptyset_0$, and at the middle of column, $\emptyset_m$, are determined. It is worth mentioning that for each step, by changing the axial load, the corresponding moment-curvature diagram was recalculated according to the mentioned process. By substituting these values into Equation 11, the deflection of mid-height of column is computed. If the latter and the assumed deflection are the same, the answer is valid, otherwise, other values for deflection should be tried until a valid answer is found as shown in Figure 7. This process begins with an initial deflection at mid-height of column, followed by an increased increment in this deflection, which defines as the displacement step. The difference between the initial deflection and the deflection calculated based on the sine function assumption, which is defined as the control value, is tracked as the initial deflection increases. There is a certain deflection at which the sign of the control value changes, which means in the current step the answer is passed. Therefore, the process of finding a valid answer is started with a smaller displacement step repeatedly until the control value is less than 10^{-10} or approaches zero. In the latter case, if the control value decreased by changing the deflection at mid height of the column, the convergence would happen and a valid answer exists, otherwise, the code cannot find a valid answer. The explained process is the second-order analysis of the column which considers the effect of initial eccentricity and the deflection caused by axial force in finding the final deflected shape of the column. The latter is applied by considering $P(e+\delta)$ as the bending moment used to find the curvatures for the iterative process, as illustrated in Figure 7.

The applied load increases in some steps, and after finding a satisfaction of convergence achieved, the values of deflection at mid-height of column, strain of GFRP rebar in compression and tension, the bending moment, and curvature are captured for each load step. This process continues up to the point that the deflections are huge enough to demand moments higher than peak moment in the moment curvature diagram. After this point, instead of increasing the load, the load will be decreased in each load step to build the descending branch using the same procedure. The critical control in this process is the record of curvature in each step; which means the curvature is not allowed to be less than the curvature in the past step. This condition helps to find the proper answer when there are two possible answers for a certain bending moment demand in moment curvature diagram for the descending branch as illustrated in Figure 7.

4.2. Verification

Using the experimental results which was presented in Section 3 of this paper, the proposed analytical model was verified. The analysis performed for three different GFRP reinforced concrete columns. The column used for verification is explained in the experimental section, however, the modulus of elasticity of GFRP bars were considered equal to 38.74 GPa for both tension and compressive bars. For the calculation of axial load-bending moment interaction diagram, the same process as finding the moment-curvature applied using Equation 1 through Equation 8, however, the strain at the furthest compressive fiber in concrete was taken 0.003 mm/mm as the point of crushing of concrete per ACI 318 [30]. Three eccentricity to width ratios of 0.1, 0.2, and 0.3 were used to analysis, and the results are shown in Figure 8. There were two sets of experimental data for each case which is reduced to one in Figure 8 by taking average of them.

In Figure 8(a), the strain of GFRP bars from strain gauges at the mid height of column in both tension and compression side are shown. The results show a good agreement between the strains predicted by the proposed model the average experimental strains. Figure 8(b) shows the moment- curvature of the column at mid-height derived from the model which is in a good agreement with average experimental values calculated using the values of strain gauges. In Fig 8(c), the load versus the displacement of the column at its mid-height is shown, where the model predicts the slope and the peak load of the experimental curves very well, and predicts the descending branch up to the point that is numerically achievable. The loading path calculated by model, as shown in Figure 8(d), are exactly the same as the ones calculated from average experimental data.

The values of peak loads as well as the values of displacement, compressive and tensile strains, moment, and curvature at the peak load derived by analytical model as well as the average of test data are presented in Table 3. It is noticed that these average values are different from average curves presented in Figure 8, since only the average of mentioned parameters were shown in Table 3. This means, if the peak loads of two specimens with the same eccentricity happens at different displacements, they are not summed in Figure 5 while the summation is presented in Table 3. Table 3 shows that model can predict the peak load and its corresponding bending moment with roughly 7% error. It is seen that as load eccentricity increases, the prediction of the values of compressive strain of GFRP bars and deflection at the mid-height of the column specimens are less accurate. Moreover, another verification considered in which load displacement behavior and rebar strains of a circular column with a diameter of 305 mm and a length of 1500 mm (slenderness ratio of 20) reinforced with eight #5 GFRP rebars of 16 mm diameter in a study performed experimentally by Hadhood et al. [14] is verified versus the model as shown in Figure

9. The cross-sectional area of each rebar was 199 mm^2 and the cover was 25 mm. The modulus of elasticity and strength of GFRP were 54.9 GPa and 1289 MPa, respectively, while the concrete strength was 35 MPa. Four pin-pin columns called C2-P2, C3-P2, C4-P2, and C5-P2 with the load eccentricity of 25,50,100,200 mm, respectively, were verified against the analytical-numerical model. Overall, the results show a good agreement between the results of the proposed model and experimental data. In the next section, using the verified model, a parametric study on important parameters is presented.

4.3. Parametric Studies

In this section, the analytical model developed in this study used to perform a parametric study. As one of goals of this study was to find out the effectiveness of GFRP bars in compression, the first subsection is assigned to compressive GFRP bars. In addition, parameters such as the reinforcement ratio, and concrete strength are considered in the following sections.

4.3.1. Effect of ignoring compressive bars

In this subsection, the analytical model was used to investigate the effects of ignoring compressive GFRP bars in the behavior of short concrete columns as suggested by major design guides/codes. The parametric study considered the cross-section and material properties introduced in verification section, but using different eccentricities. As it is presented in Figure 10, there is no significant difference in the load deflection behavior and loading path between considering GFRP bars in compression or neglecting them. However, the interaction diagram shows higher axial capacities using the compressive layer of GFRP bars. Table 4 provides the results of the analysis, including the axial and the corresponding bending moment capacities of columns determined by the analytical model, once with considering GFRP bars in compression, and once by neglecting them. For all cases, the axial and bending moment capacities at peak load are higher when GFRP rebar is considered in the calculation which proves the effectiveness of compressive GFRP bars. In addition, the axial and bending moment capacities of the columns at strain of 0.003 mm/mm, which is used for design purpose suggested by ACI [30], approaches to the same values when compression rebar exists or not as the load eccentricity reaches higher values. As presented in Table 4. This means that the calculation of column capacity is not different by considering compressive GFRP bars in higher eccentricities.

4.3.2. Effect of reinforcement ratio

To investigate the effect of reinforcement ratio in the compressive strain of GFRP bars, a parametric study consisting of eight reinforcement ratios of 1.27, 1.90, 2.25, 3.38, 3.52, 5.07, 5.28, and 7.60% (4#3, 6#3, 4#4, 6#4, 4#5, 4#6, 6#5, and 6#6) were considered. In addition, the columns in three eccentricity to width ratios of 0.1, 0.2, and 0.3 were examined, and all other parameters were the same as the ones used for the model verification. The corresponding compressive strain at peak load are presented in Figure 11. The results show that as the reinforcement ratio increases, the strain in compressive rebar increases for all eccentricities, however, their values at peak load does not reach even half of the proportional limit which was introduced in Section 2.2 of this study. The results confirm the compressive strains sustained by the GFRP bars cannot lead to crushing of bars in compression.

4.3.3. Effect of concrete strength

In this subsection, a parametric study was performed to reveal the effect of concrete strength on the behavior of compressive GFRP bars. Thirteen concrete strength of 20, 25, 30, 35, 40, 45, 50, 55, 60, 65, 70, 75, and 80 MPa were examined with three eccentricity to width ratios of 0.1, 0.2, and 0.3 while all other parameters were kept unchanged and the same as verification section. The results including the compressive strain at peak load, and where available, the ones at 85 percent drop after peak load are presented in Figure 12. The results show that by increasing the concrete strength the compressive strain of GFRP increases in all eccentricities. Again, the results at peak load and 0.85 of peak load show that the compressive strains do not reach their critical value, and in turn, do not cause catastrophic damage in GFRP bars.

4.3.4. Effect of modulus of elasticity of GFRP bars

The effect of modulus of elasticity of GFRP bars on the behavior of compressive GFRP bars were also evaluated using eleven different values ranging from 30 to 80 GPa by analyzing the same model used in verification part and with three eccentricity to width ratios of 0.1, 0.2, and 0.3. The strain of GFRP bars in compression at peak load and 0.85 of peak load, which is recorded at mid-height of specimens, for various modulus of elasticities of GFRP bars and diverse load eccentricities are presented in Figure 13. For all eccentricity to width ratios, as modulus of elasticity of GFRP bars increases, the compressive strain of bars at peak load slightly decreases while this value at 85% of peak load is approximately constant, as shown in Figure 13. It is observed that the values of compressive strain of GFRP at peak load and 0.85 of peak load are getting closer as eccentricity increases. Similar to other subsections, no damage due to compressive failure of GFRP is expected at peak load and 0.85 of peak load since the strain values are far below the crushing strength of GFRP bars.

5. CONCLUSION

In this study, the performance of short concrete columns reinforced with GFRP bars were investigated experimentally and analytically. A total of fourteen column specimens including nine reinforced and five plain specimens were tested under four load eccentricity to width ratios of 0, 0.1, 0.2, and 0.3. Moreover, an analytical model was developed and verified with test results, and a parametric study was performed using the model. The following conclusions can be drawn:

- Based on coupon tests, the modulus of elasticity of GFRP bars used in this study were close in tension and compression, and the strength in compression was even higher than in tension.
- No buckling or crushing of GFRP bars in compression were observed during the test before the failure of specimens.
- The average of experimental compressive strain of GFRP bars, read from strain gauges after failure of specimens, were 22% and 16% of the ultimate capacity of bars in compression, derived from coupon test, and were 36% and 25% of the proportional limit of 0.0133 mm/mm. In other words, even the 50% of capacity of compressive GFRP bars were not reached in the tests.
- The proposed analytical model showed very good agreement with the experimental results. The model predicted the peak load of the test specimens with an average error of less than 7%.
- The parametric study revealed that the capacity of column by considering GFRP bars in compression or neglecting them is similar up to the defined crushing strain of concrete 0.003 mm/mm, however there is a gain in capacity at the peak load which requires higher strains; even experimental results did not reach their peak load at 0.003 mm/mm which is compatible with the numerical model.
- Based on the results of the parametric study, it was observed that the values of compressive strain of GFRP bars in compression at peak load and even the compressive strain at 85% of peak load (after peak) did not reach 50% of crushing strain of GFRP bar. From design

point of view, for the limited parameters considered in this study, this paper suggests to consider GFRP bars in compression as linear elastic materials until concrete reached to its compressive strain limit of 0.003 mm/mm. However, more studies are required to give a design suggestion such as risk assessment study and more comprehensive experimental program considering more variability in parameters.

Overall, for the selected set of tests and parametric study which has performed in this study, the contribution of GFRP bars in compression can be considered in the design of GFRP reinforced short concrete columns and its ignorance in design guidelines is conservatively recommended.

6. ACKNOWLEDGEMENT

Authors would like to thank Blair Nickerson, Brian Kennedy, Jesse Keane, and Brian Liekens and for their assistance in the lab. The authors would also like to acknowledge and thank NSERC and Dalhousie University for their financial support.

7. REFERENCES

[1] P. K. Mallick, Fiber Reinforced Composites Materials, Manufacturing, and Design, Boca Raton, Florida: CRC Press, 2008.

[2] A. De Luca, F. Matta and A. Nanni, "Behavior of Full-Scale Glass Fiber-Reinforced Polymer Reinforced Concrete Columns under Axial Load," *ACI Structural Journal*, vol. 107, no. 5, pp. 589-596, 2010.

[3] S. H. Alsayed, "Flexural behaviour of concrete beams reinforced with GFRP bars," *Cement and Concrete Composites,* vol. 20, no. 1, pp. 1-11, 1998.

[4] H. A. Toutanji and M. Saafi, "Flexural behavior of concrete beams reinforced with glass fiber-reinforced polymer (GFRP) bars," *ACI Structural Journal,* vol. 97, no. 5, pp. 712-719, 2000.

[5] M. Thériault and B. Benmokrane, "Effects of FRP Reinforcement Ratio and Concrete Strength on Flexural Behavior of Concrete Beams," *Journal of Composites for Construction,* vol. 2, no. 1, pp. 7-16, 1998.

[6] D. H. Deitz, . I. E. Harik and H. Gesund, "One-Way Slabs Reinforced with Glass Fiber Reinforced Polymer Reinforcing Bars," *ACI Special Publication,* vol. 188, pp. 279-286, 1999.

[7] A. El-sayed, E. El-Salakawy and B. Benmokrane, "Shear Strength of One-Way Concrete Slabs Reinforced with Fiber-Reinforced Polymer Composite Bars," *Journal of Composites for Construction*, vol. 9, no. 2, pp. 147-157, 2005.

[8] C. R. Michaluk, S. H. Rizkalla, G. Tadros and B. Benmokrane, "Flexural Behavior of One-Way Concrete Slabs Reinforced by Fiber Reinforced Plastic Reinforcements," *ACI Structural Journal,* vol. 95, no. 3, pp. 353-365, 1998.

[9] B. Benmokrane, E. El-Salakawy, A. El-Ragaby and T. Lackey, "Designing and Testing of Concrete Bridge Decks Reinforced with Glass FRP Bars," *Journal of Bridge Engineering,* vol. 11, no. 2, pp. 217-229, 2006.

[10] A. C. Berg , L. C. Bank, M. G. Olivia and J. S. Russell, "Construction and cost analysis of an FRP reinforced concrete bridge deck," *Construction and Building Materials,* vol. 20, no. 8, pp. 515-526, 2006.

[11] N. Galati, G. Tumialan and A. Nanni, "Strengthening with FRP bars of URM walls subject to out-of-plane loads," *Construction and Building Materials,* vol. 20, no. 1, pp. 101-110, 2006.

[12] H. R. Hamilton Iii and C. W. Dolan, "Flexural capacity of glass FRP strengthened concrete masonry walls," *Journal of Composites for Construction,* vol. 5, no. 3, pp. 170-178, 2001.

[13] M. Z. Afifi, H. M. Mohamed and B. Benmokrane, "Strength and Axial Behavior of Circular Concrete Columns Reinforced with CFRP Bars and Spirals," *Journal of Composites for Construction,* vol. 18, no. 2, p. 04013035, 2013.

[14] A. Hadhood, H. M. Mohamed, F. Ghrib and B. Benmokrane, "Efficiency of glass-fiber reinforced-polymer (GFRP) discrete hoops and bars in concrete columns under combined axial and flexural loads," *Composites Part B,* vol. 114, pp. 223-236, 2017.

[15] M. N. S. Hadi and J. Youssef, "Experimental Investigation of GFRP-Reinforced and GFRP-Encased Square Concrete Specimens under Axial and Eccentric Load, and Four-Point Bending Test," *Journal of Composites for Construction,* vol. 20, no. 5, p. 04016020, 2016.

[16] T. A. Hales, C. P. Pantelides and L. D. Reaveley, "Experimental Evaluation of Slender High-Strength Concrete Columns with GFRP and Hybrid Reinforcement," *Journal of Composites for Construction,* vol. 20, no. 6, p. 04016050, 2016.

[17] T. Jiang and . J. Teng, "Theoretical model for slender FRP-confined circular RC columns," *Construction and Building Materials,* vol. 32, pp. 66-76, 2012.

[18] H. J. Zadeh and . A. Nanni, "Design of RC Columns Using Glass FRP Reinforcement," *Journal of Composites,* vol. 17, no. 3, pp. 294-304, 2013.

[19] A. Mirmiran, W. Yuan and X. Chen, "Design of Slenderness in Concrete Columns Internally Reinforced with Fiber-Reinforced Polymer Bars," *ACI structural Journal,* vol. 98, no. 1, pp. 116-125, 2001.

[20] ACI 440.1R, Guide for the Design and Construction of Structural Concrete Reinforced Fiber-Reinforced Polymer (FRP) Bars, Farmington Hills, MI: American Concrete Institute, 2015.

[21] CAN/CSA S806-12, Design and construction of building structures with fibre-reinforced polymers, Canadian Standards Association, 2012.

[22] Fib Bulletin 40, "FRP Reinforcement in RC structures," the International Federation for Structural Concrete, Stuttgart, 2007.

[23] C. C. Choo, I. E. Harik and H. Gesund, "Strength of Rectangular Concrete Columns Reinforced with Fiber-Reinforced Polymer Bars," *ACI Structural Journal*, vol. 103, no. 3, pp. 452-459, 2006.

[24] H. Tobbi, A. S. Farghaly and B. Benmokrane, "Concrete Columns Reinforced Longitudinally and Transversally with Glass Fiber-Reinforced Polymer Bars," *ACI Structural Journal*, vol. 109, no. 4, pp. 551-558, 2012.

[25] H. M. Mohamed, M. Z. Afifi and B. Benmokrane, "Performance Evaluation of Concrete Columns Reinforced Longitudinally with FRP Bars and Confined with FRP Hoops and

Spirals under Axial Load," *Journal of Bridge Engineering,* vol. 19, no. 7, p. 04014020, 2014.

[26] K. Khorramian and P. Sadeghian, "Short Concrete Columns Reinforced with GFRP Rebars under Eccentric Loading," in *CSCE - Leadership in Sustainable Infrastructure*, Vancouver, Canada, 2017.

[27] B. Fillmore and P. Sadeghian, "Compressive Behavior of Concrete Cylinders Reinforced with Glass Fiber Reinforced Polymer Bars," in *CSCE - Leadership in Sustainable Infrastructures*, Vancouver, Canada, 2017.

[28] ASTM D7205/D7205M-06, Standard Test Method for Tensile Properties of Fiber Reinforced Polymer Matrix Composite Bars, West Conshohocken, PA: American Society for Testing and Materials, 2011.

[29] Q. S. Khan, M. N. Sheikh and M. N. S. Hadi, "Tension and compression testing of fibre reinforced polymer (FRP) bars," in *Joint Conference of the 12th International Symposium on Fiber Reinforced Polymers for Reinforced Concrete Structures (FRPRCS-12) & the 5th Asia-Pacific Conference on Fiber Reinforced Polymers in Structures (APFIS-2015),* Wollongong, New South Wales, Australia, 2015.

[30] ACI 318-14, Building Code Requirements for Structural Concrete, Farmington Hills, MI: American Concrete Institute, 2014.

[31] E. Hognestad, "A Study of Combined Bending and Axial Load in Reinforced Concrete Members," *Bulletin 399,* p. 128, 1951.

[32] S. Popovics, "A Numerical Approach to the Complete Stress-Strain Curve of Concrete," *Cements and Concrete Research,* vol. 3, no. 5, pp. 583-599, 1973.

[33] J. K. Wight and J. G. MacGregor, Reinforced Concrete Mechanics and Design, Upper Saddle River, NJ: Pearson Education Inc, 2012.

[34] B. Broms and I. M. Viest, "Long Reinforced Concrete Columns: A symposium," *Transactions, ASCE,* vol. 126, no. 2, pp. 308-400, 1961.

[35] N. A. Lloyd and B. V. Rangan, "Studies on High-Strength Concrete Columns under Eccentric Compression," *ACI Structural Journal,* vol. 93, no. 6, pp. 631-638, 1996.

[36] C. Claeson and K. Gylltoft, "Slender High-Strength Concrete Columns Subjected to Eccentric Loading," *Journal of Structural Engineering,* vol. 124, no. 3, pp. 233-240, 1998.

[37] P. Sadeghian, A. R. Rahai and M. R. Ehsani, "Experimental Study of Rectangular Columns Strengthened with CFRP Composites under Eccentric Loading," *Journal of Composites for Construction,* vol. 14, no. 4, pp. 443-450, 2010.

[38] P. Sadeghian and A. Fam, "Strengthening Slendnder Reinforced Concrete Columns Using High-Modulus Longitudinal Reinforcement for Buckling Control," *Journal of Structural Engineering, ASCE,* vol. 141, no. 4, p. 04014127, 2015.

[39] A. Mirmiran, W. Yuan and X. Chen, "Design of Slenderness in Concrete Columns Internally Reinforced with Fiber-Reinforced Polymer Bars," *ACI Structural Journal,* vol. 98, no. 1, pp. 116-125, 2001.

Table 1. Test matrix

No.	Specimen ID	Eccentricity (mm)	Eccentricity ratio	Reinforcement
1	R-e0-1	0	0	GFRP
2	R-e0-2	0	0	GFRP
3	R-e10-1	15	0.1	GFRP
4	R-e10-2	15	0.1	GFRP
5	R-e10-3	15	0.1	GFRP
6	R-e20-1	30	0.2	GFRP
7	R-e20-2	30	0.2	GFRP
8	R-e30-1	45	0.3	GFRP
9	R-e30-2	45	0.3	GFRP
10	P-e0-1	0	0	Plain
11	P-e0-2	0	0	Plain
12	P-e10-1	15	0.1	Plain
13	P-e10-2	15	0.1	Plain
14	P-e10-3	15	0.1	Plain

Table 2. Summary of test results

Specimen group	Peak Load, P_u (kN)	Rebar strain at P_u (mm/mm)	Rebar strain at P_u to prop. limit	Rebar strain at P_u to crush. strain	Rebar strain at $0.85P_u$ (mm/mm)	Rebar strain at $0.85P_u$ to prop. limit	Rebar strain at $0.85P_u$ to crush. strain	Failure mode
P-e0	719.2	-	-	-	-	-	-	CS → CD
R-e0	774.9	0.00275	0.21	0.14	0.00459	0.35	0.24	CC → CS
P-e10	596.3	-	-	-	-	-	-	CS → CD
R-e10	692.8	0.00279	0.21	0.15	0.00416	0.31	0.22	CC → CS
R-e20	578.2	0.00289	0.22	0.15	0.00472	0.36	0.25	CC → CS
R-e30	354.1	0.00361	0.27	0.19	0.00588	0.45	0.31	CC → CS
Average	-	-	0.23	0.16	-	0.36	0.25	-

Note: The results are average of identical specimens. Rebar strain recorded by SG2 (see Figure 3) installed on the middle rebar at the extreme compressive layer; 0.85Pu is related to post peak; NA: not available; CC: concrete crushing; CS: concrete spalling; CD: concrete destruction; prop. limit = 0.0133 mm/mm; crush. strain = 0.0190 mm/mm.

Table 3. Comparison of model and experimental results

Characteristic	e/h (%)	Test	Model	Error (%)	Absolute Error (%)
Peak Load (kN)	10	692.8	667.7	3.62	6.73±6.20
	20	578.2	498.0	13.87	
	30	354.1	363.7	-2.7	
Lateral mid-height displacement at peak load (mm)	10	0.92	0.67	27.18	26.82±8.77
	20	1.11	0.91	17.87	
	30	2.03	1.31	35.4	
Compressive bar strain at peak load (mm/mm)	10	-0.00279	-0.00256	8.28	20.80±14.14
	20	-0.00289	-0.00237	17.98	
	30	-0.00360	-0.00230	36.14	
Tensile bar strain at peak load (mm/mm)	10	-0.00072	-0.00069	3.49	52.19±70.87
	20	0.00008	0.00019	-133.5	
	30	0.00117	0.00140	-19.58	
Moment at peak load (kN-m)	10	11.00	10.46	4.88	6.74±7.00
	20	18.00	15.39	14.48	
	30	16.70	16.84	-0.85	
Curvature at peak load (1/km)	10	20.85	22.19	-6.43	5.58±3.44
	20	29.91	30.44	-1.79	
	30	48.12	44.03	8.51	

Note: e/h is the load eccentricity to width ratio.

Table 4. Comparison of axial load and corresponding bending moment capacities with and without compressive bars based on parametric study

e/h (%)	@ compressive strain of 0.003						@ Peak load					
	Axial load (kN)			Bending moment (kN-m)			Axial load (kN)			Bending moment (kN-m)		
	with comp. rebar	W/O comp. rebar	Diff. (%)	with comp. rebar	W/O comp. rebar	Diff. (%)	with comp. rebar	W/O comp. rebar	Diff. (%)	with comp. rebar	W/O comp. rebar	Diff. (%)
0	898.9	856.9	4.67	-	-	-	908.7	870.6	4.19	-	-	-
5	762.4	744.4	2.35	6.09	5.87	3.70	762.5	744.4	2.37	6.10	5.87	3.84
10	664.8	645.9	2.85	10.37	10.04	3.23	667.7	645.9	3.27	10.46	10.04	4.07
15	579.4	565.2	2.46	13.44	13.07	2.71	581.8	565.2	2.87	13.54	13.07	3.41
20	495.1	486.3	1.76	15.25	14.95	2.00	498.0	486.3	2.34	15.39	14.95	2.92
25	420.4	415.7	1.11	16.15	15.95	1.22	424.5	415.7	2.07	16.37	15.95	2.56
30	357.0	355.1	0.51	16.44	16.34	0.62	363.7	355.8	2.17	16.84	16.39	2.71
35	306.1	305.5	0.19	16.43	16.38	0.30	315.9	307.6	2.64	17.08	16.53	3.23
40	266.1	266.1	-0.01	16.31	16.30	0.08	279.1	270.0	3.29	17.26	16.58	3.94
45	234.7	234.9	-0.10	16.17	16.17	-0.02	250.5	240.4	4.03	17.44	16.61	4.76
50	209.7	209.9	-0.07	16.04	16.04	0.00	227.8	216.9	4.78	17.64	16.65	5.63
60	172.8	173.0	-0.13	15.83	15.85	-0.08	195.3	181.8	6.90	18.24	16.73	8.27
80	128.3	128.3	0.03	15.63	15.62	0.06	151.9	138.1	9.06	18.79	16.90	10.09
100	102.2	102.1	0.07	15.53	15.52	0.09	124.2	111.8	9.96	19.12	17.07	10.75

Note: e/h is the load eccentricity to width ratio; “comp.”, “Diff.”, and “W/O” are used in the table instead of “compressive”, “Difference”, and “without”, respectively.

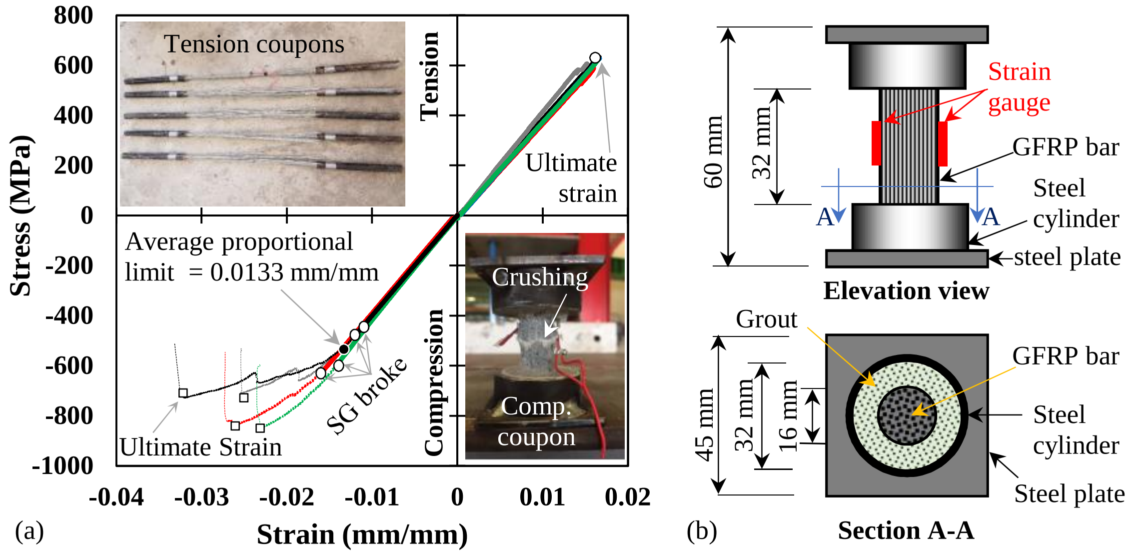

Figure 1. Material test: (a) Stress-strain curves of GFRP bars in tension and compression; and (b) schematic drawing of GFRP bar coupon for compression test.

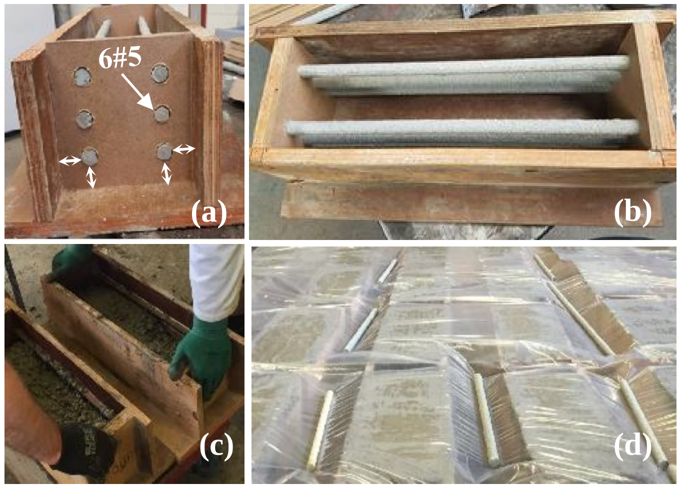

Figure 2. Specimen fabrication: (a) cross section; (b) top view; (c) casting; and (d) curing.

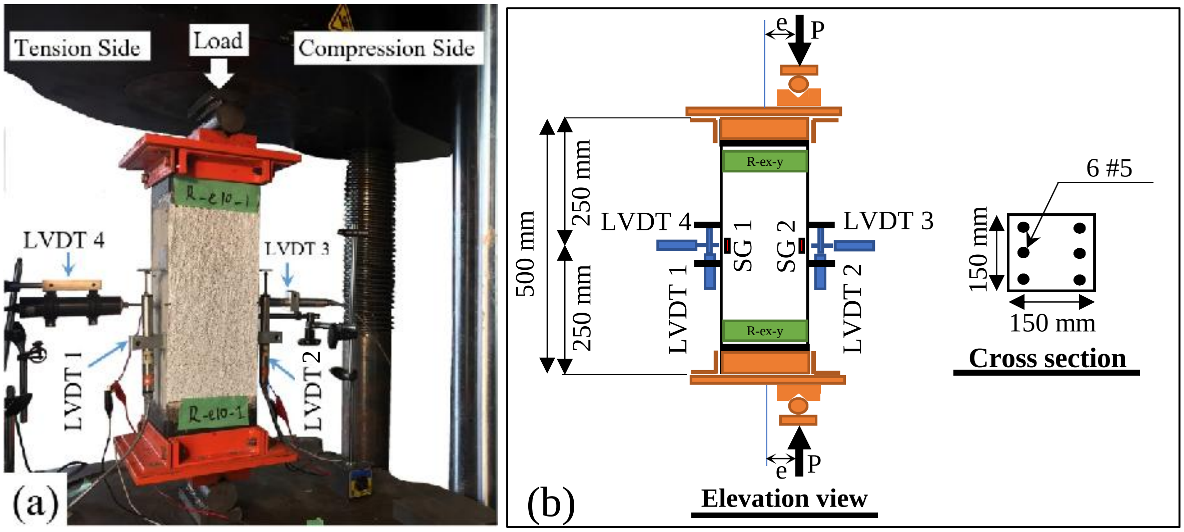

Figure 3. Test set up and instrumentation: (a) testing machine and instrumentation, and (b) schematic testing specimen and reinforcement layout

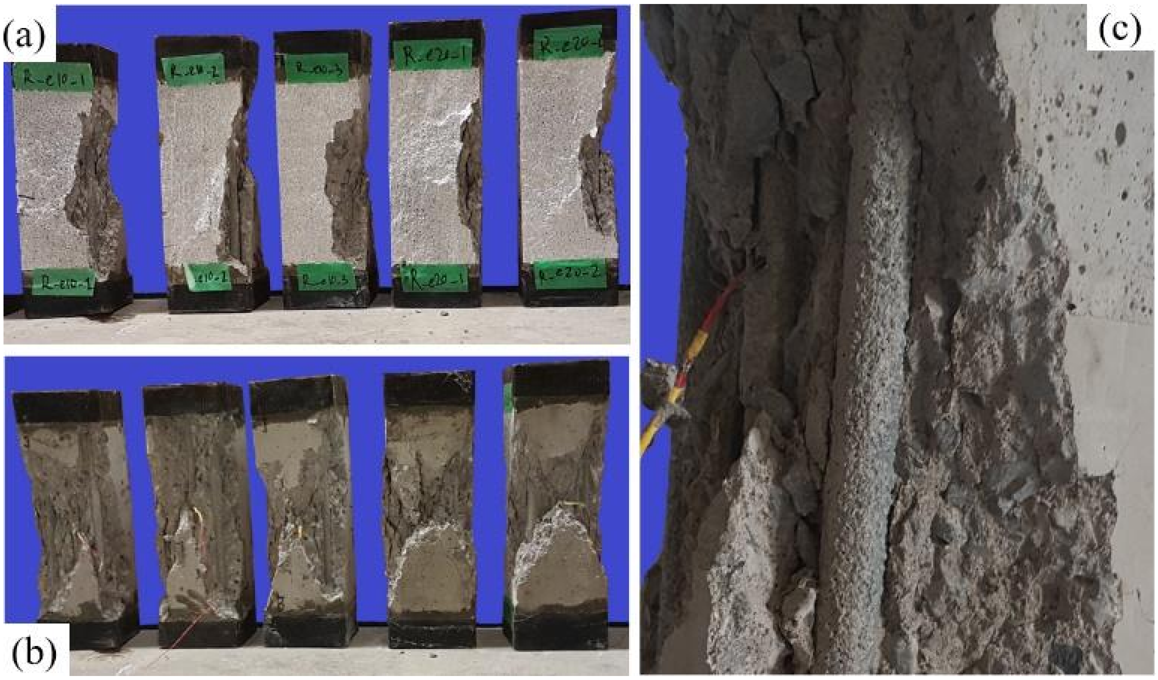

Figure 4. Mode of failures: (a) side view; (b) compression side; and (c) crushed concrete and visually intact compressive rebar.

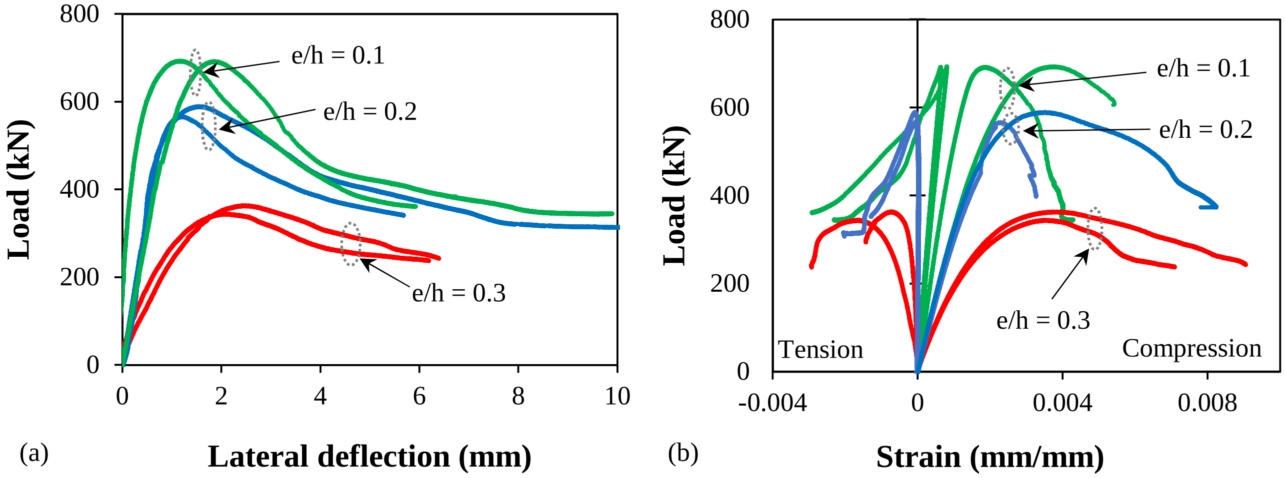

Figure 5. Test results: (a) axial load vs. lateral displacement of specimens at mid-height; and (b) axial load vs. strain of compressive and tensile GFRP bars.

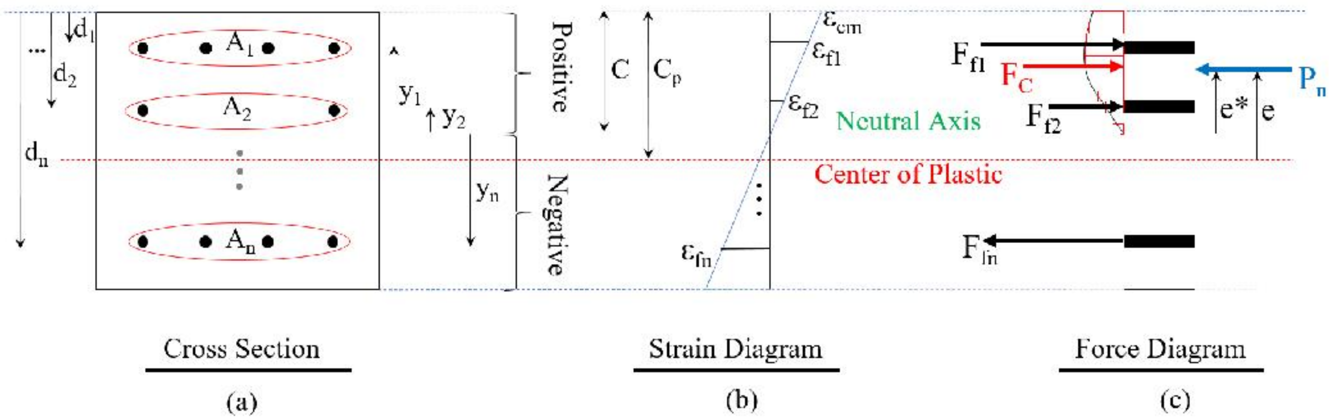

Figure 6. Mechanism of cross-sectional analytical model: (a) section definitions; (b) strain diagram; and (c) force diagram.

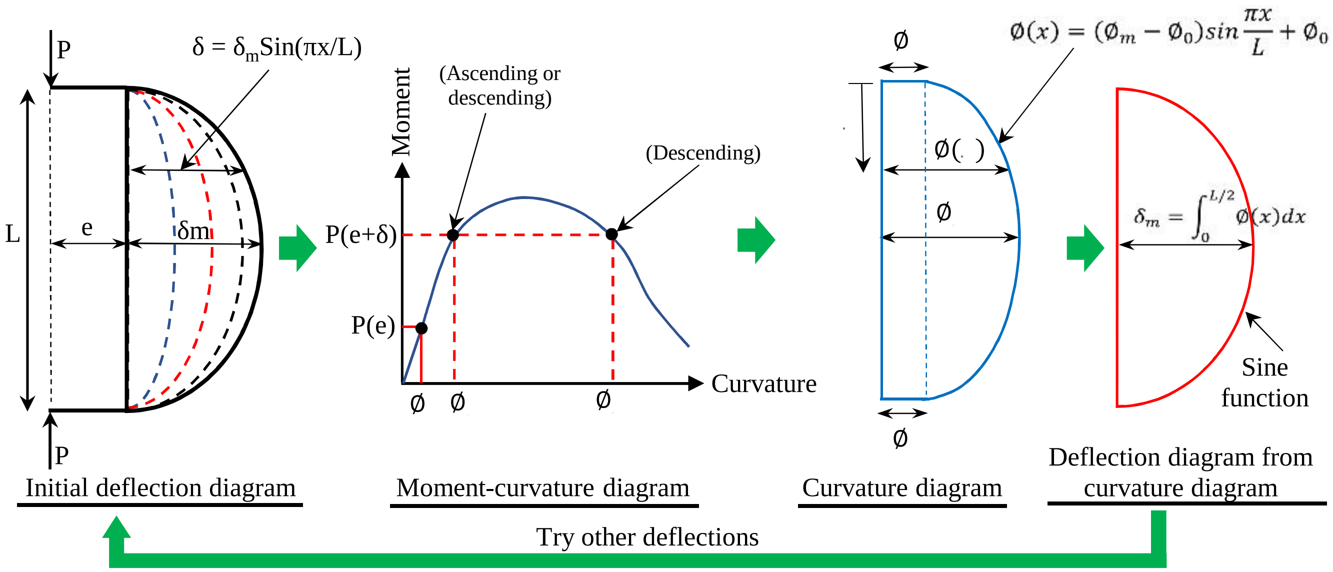

593

594 **Figure 7. Schematic iteration process for finding deflection at mid height of column.**

595

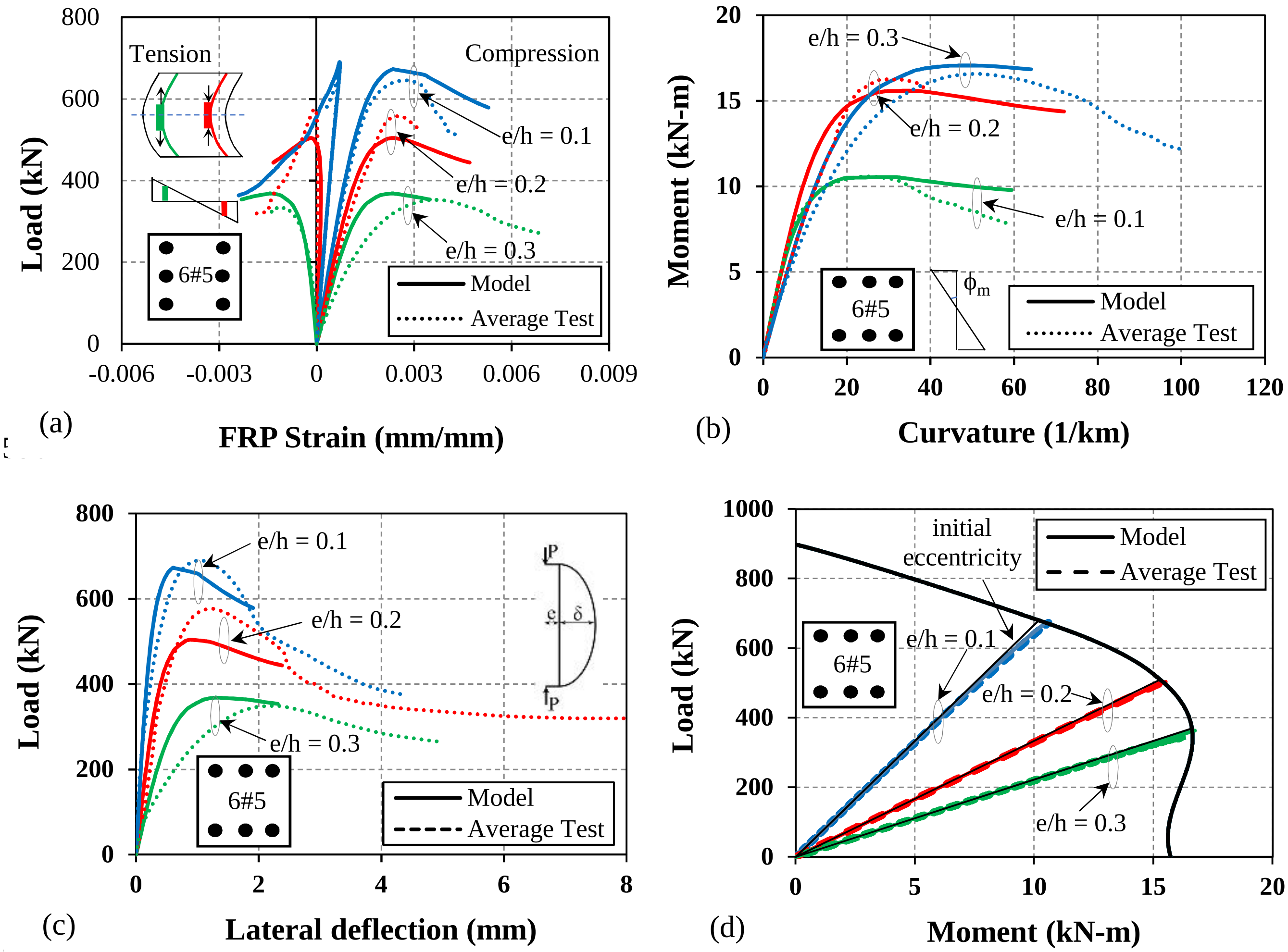

Figure 8. Model verification: (a) axial load vs. strain of compressive and tensile GFRP bars at the mid height; (b) moment vs. curvature diagram at the mid-height; (c) axial load vs. lateral displacement of specimens at the mid-height; and (d) axial load vs. bending moment interaction diagram and loading path curves.

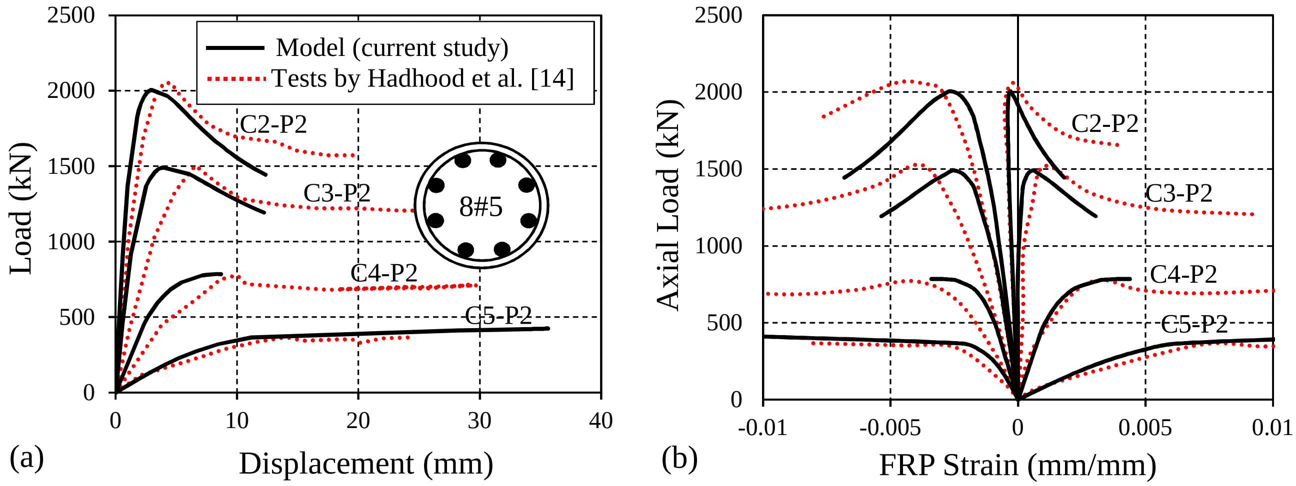

Figure 9. Model verification with circular GFRP reinforced concrete column tested by Hadhood et al. [14]: (a) axial load vs. lateral displacement of specimens at mid-height; and (b) axial load vs. strain of compressive and tensile GFRP bars at the mid-height.

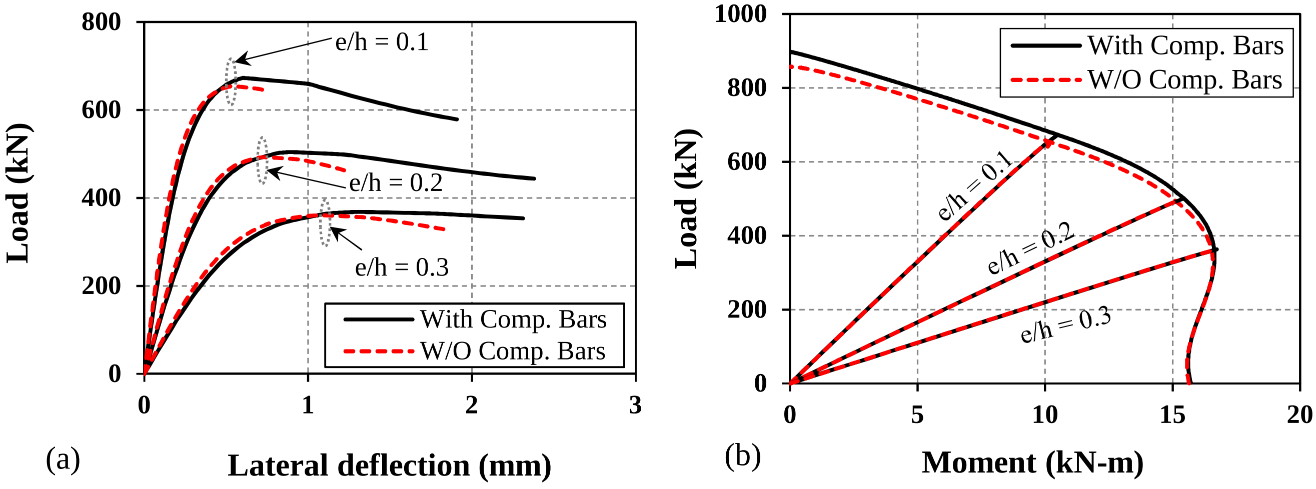

Figure 10. Compressive rebar effect: (a) axial load vs. lateral displacement of specimens at mid-height; and (b) axial load vs. bending moment interaction diagram and loading path.

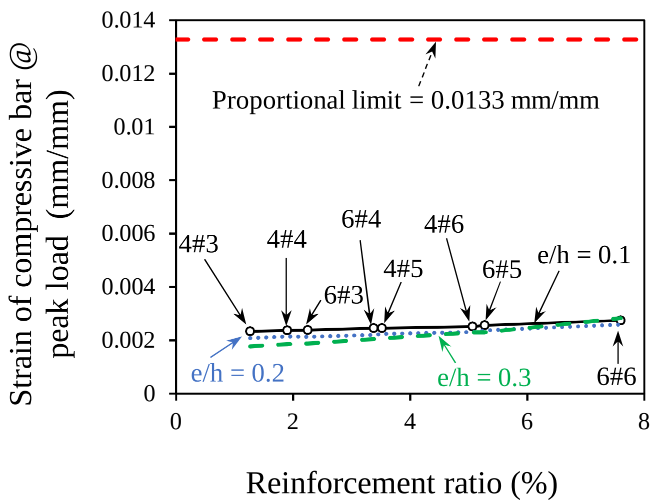

Figure 11. Effect of reinforcement ratio on strain of compressive GFRP bars.

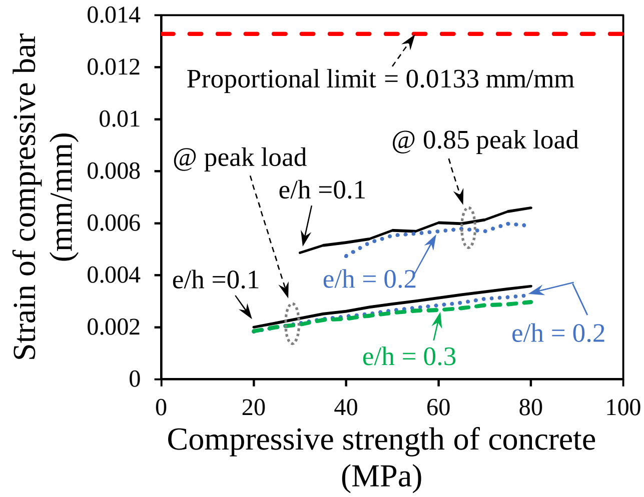

Figure 12. Effect of compressive strength of concrete on strain of compressive GFRP bars.

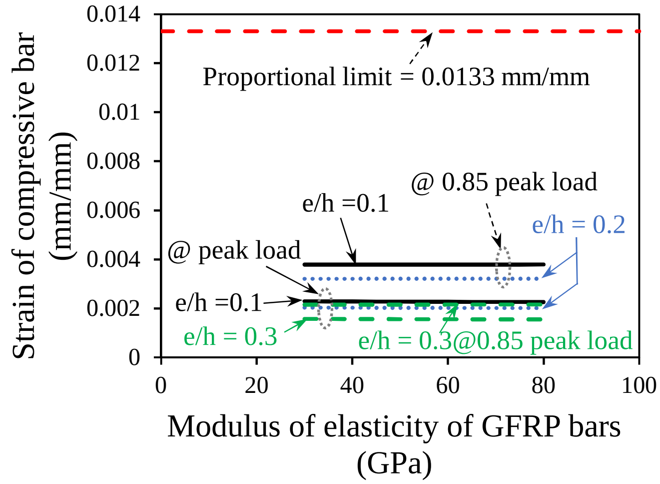

Figure 13. Effect of modulus of elasticity of GFRP bars on strain of compressive bars.